AGU PUBLICATIONS

Earth's Future

RESEARCH ARTICLE
10.1002/2015EF000347

Special Section:
Integrated field analysis & modeling of the coastal dynamics of sea level rise in the northern Gulf of Mexico

Dynamic simulation and numerical analysis of hurricane storm surge under sea level rise with geomorphologic changes along the northern Gulf of Mexico

Matthew V. Bilskie[1], S. C. Hagen[2], K. Alizad[3], S. C. Medeiros[3], D. L. Passeri[4], H. F. Needham[5], and A. Cox[6]

[1]Department of Civil and Environmental Engineering, Louisiana State University, Baton Rouge, Louisiana, USA, [2]Department of Civil and Environmental Engineering, Center for Computation and Technology, Louisiana State University, Baton Rouge, Louisiana, USA, [3]Department of Civil, Environmental, and Construction Engineering, University of Central Florida, Orlando, Florida, USA, [4]U.S. Geological Survey St. Petersburg Coastal and Marine Science Center, Saint Petersburg, Florida, USA, [5]Marine Weather and Climate, Baton Rouge, Louisiana, USA, [6]Oceanweather Inc., Cos Cob, Connecticut, USA

Abstract This work outlines a dynamic modeling framework to examine the effects of global climate change, and sea level rise (SLR) in particular, on tropical cyclone-driven storm surge inundation. The methodology, applied across the northern Gulf of Mexico, adapts a present day large-domain, high resolution, tide, wind-wave, and hurricane storm surge model to characterize the potential outlook of the coastal landscape under four SLR scenarios for the year 2100. The modifications include shoreline and barrier island morphology, marsh migration, and land use land cover change. Hydrodynamics of 10 historic hurricanes were simulated through each of the five model configurations (present day and four SLR scenarios). Under SLR, the total inundated land area increased by 87% and developed and agricultural lands by 138% and 189%, respectively. Peak surge increased by as much as 1 m above the applied SLR in some areas, and other regions were subject to a reduction in peak surge, with respect to the applied SLR, indicating a nonlinear response. Analysis of time-series water surface elevation suggests the interaction between SLR and storm surge is nonlinear in time; SLR increased the time of inundation and caused an earlier arrival of the peak surge, which cannot be addressed using a static ("bathtub") modeling framework. This work supports the paradigm shift to using a dynamic modeling framework to examine the effects of global climate change on coastal inundation. The outcomes have broad implications and ultimately support a better holistic understanding of the coastal system and aid restoration and long-term coastal sustainability.

Key Points:
- A dynamic storm surge modeling framework is presented
- Shoreline morphology, marsh migration and LULC is incorporated into the storm surge model
- Storm surge under sea level rise is highly dynamic

Corresponding author:
M. V. Bilskie, matt.bilskie@gmail.com

Citation:
Bilskie, M. V., S. C. Hagen, K. Alizad, S. C. Medeiros, D. L. Passeri, H. F. Needham, and A. Cox (2016), Dynamic simulation and numerical analysis of hurricane storm surge under sea level rise with geomorphologic changes along the northern Gulf of Mexico, *Earth's Future*, *4*, 177–193, doi:10.1002/2015EF000347.

Received 15 DEC 2015
Accepted 14 MAR 2016
Accepted article online 4 APR 2016
Published online 9 MAY 2016

1. Introduction

A byproduct of a warming climate is sea level rise (SLR), which is mainly caused by thermal expansion of the sea and ice loss [*Parris et al.*, 2012]. Long-term tide gage records show that global mean sea levels have risen 1.7 ± 0.3 mm/yr over the last century [*Church and White*, 2006; *Holgate*, 2007]. Since 1993, satellite altimetry data have recorded an increase to 3.3 ± 0.4 mm/yr [*Ablain et al.*, 2009; *Nicholls and Cazenave*, 2010]. These are global means, however, and the tide and satellite altimetry data indicate large spatial and regional variations across the Earth, with some areas experiencing up to three times the global average. Regional SLR trends are dominated by local circulation and a redistribution of heat, salinity, and water mass [*Cazenave and Cozannet*, 2014].

Estimates of the magnitude and rates of future sea levels are based on potential carbon emission scenarios, and are constructed from different assessments of ocean warming and ice sheet loss. Regardless of the methods and emission scenarios used to estimate future sea levels, the consensus is that sea levels are rising and its rate is expected to accelerate [*Jevrejeva et al.*, 2010; *Parris et al.*, 2012; *Intergovernmental Panel of Climate Change*, 2013]. *Parris et al.* [2012] derived four SLR scenarios spanning 0.2–2.0 m for the year 2100 based on different contributions of carbon emissions and ice sheet loss. The continued rise and acceleration of global sea level put low-lying coastal regions at risk with increases in frequency and magnitude of flooding [*Cazenave and Cozannet*, 2014]. Increased flooding because of SLR, in addition to regions that experience storm surges from tropical cyclones further increases the vulnerability of inundation in coastal regions.

Storm surge models, which vary in complexity and computational efficiency, are commonly used to estimate maximum water levels caused by tropical cyclones. Physics-based storm surge models require a variety of inputs such as topography, bathymetry, and bottom friction as well as astronomical tide and meteorological forcings. The benefits of hydrodynamic storm surge models are that they allow for analysis of regions that have little observational hydrodynamic data, and permit varying scenarios and changes to the input data. As described in this work, it is useful to project coastal flooding under a variety of potential climate change scenarios. The hydrodynamic models also allow for a more detailed analysis of the nonlinear interactions of storm surge and SLR [*Bilskie et al.*, 2014], and permit more accurate assessments than static, or "bathtub," modeling techniques that are not always straightforward to apply [*Hagen and Bacopoulos*, 2012; *Zhang et al.*, 2013].

McInnes et al. [2009] outlined three general methodologies to examine potential impacts of flood risk under a changing climate that employ hydrodynamic models: direct nesting approach, perturbed historical baseline approach, and the statistical dynamic approach. The direct nesting approach considers model forcing from global or regional climate models. This method is computationally expensive and heavily reliant on the accuracy of the climate model used [*Knutson and Tuleya*, 2004; *Woth et al.*, 2006]. The perturbed historical approach is similar to the direct nesting approach, however, the model is forced with historical extreme sea level events to obtain a baseline and then changes to mean sea level and hurricane intensity, for example, are included in the model simulations [*Bernier et al.*, 2007; *Atkinson et al.*, 2013; *Ding et al.*, 2013; *Zhang et al.*, 2013; *Yang et al.*, 2014; *Orton et al.*, 2015]. This method is more computationally efficient than the direct nesting approach and permits variations of multiple climate change scenarios. However, it depends upon a rich meteorological history to develop a population of extreme sea levels and in many cases flood risk is only assessed through a selected few events. In the statistical dynamic approach, a statistical model is employed to generate a population of potential storms used to force a hydrodynamic model [*McInnes et al.*, 2003; *Resio et al.*, 2009; *Mousavi et al.*, 2011; *Hagen and Bacopoulos*, 2012; *Lin et al.*, 2012]. This method performs well in regions with limited meteorological records [*McInnes et al.*, 2009]. Regardless of the applied approach, the model solution is only as good as the input data. To this end, it is of critical importance to evaluate the model's numerical description of nature and how the landscape may change in the future under normal or climate change conditions. This includes changes to the coastal landscape such as shoreline morphology, marsh migration, and land use.

Ali [1999] performed one of the first studies that examined the combined effect of storm surge with an emphasis on SLR, coastal morphology, and a change in hurricane intensity. They forced a GCOM2D hydrodynamic model with 489 individual events based on an increase in sea surface temperature of 2°C and 4°C and a SLR of 0.2 and 1.0 m to evaluate the climate change impact on storm tide return periods along the southeastern Australia coastline. *Wang et al.* [2012] employed the MIKE21 hydrodynamic model to evaluate coastal flood risk under SLR and land subsidence in Shanghai, China for the years 2030, 2050, and 2100 to provide data and suggestions for coastal protection design. *Mousavi et al.* [2011] estimated the increase in storm surge flooding for Corpus Christi, Texas for the years 2030 and 2080. The model was forced by 23 hurricane scenarios based on three historical storms (Bret, Beulah, and shifted Carla) that were selected from numerical simulations derived from surge response functions. Studies like *Atkinson et al.* [2013] and *Smith et al.* [2010] began to include waves into the computation of storm surge and SLR in addition to introducing changes to bottom friction based on new regions exposed to daily tidal flooding. *Smith et al.* [2010] demonstrated that in regions of maximum storm surge, the additional surge was equal to the SLR, but in wetland fronted areas, the storm surge was highly nonlinear and surge heights increased by 1 – 3 m in addition to the change in sea level. *Atkinson et al.* [2013] concluded that there is not a "one-size-fits-all" approach to storm surge under SLR because it is highly dependent on storm characteristics and the local geography. These studies advanced the modeling of hurricane storm surge and SLR using a dynamic modeling framework.

Bilskie et al. [2014] showed that hurricane storm surge flooding under SLR is a complex nonlinear process and changes to the coastal landscape for past and future scenarios can amplify storm surge by 80% or reduce storm surge by 100%, relative to the amount of SLR. They found that altering the coastal floodplain topographic elevations, including barrier island morphology, and incorporating changes in land use land cover (LULC) based on past conditions and future scenarios altered the path, pattern, and magnitude of flooding. From this work, the normalized nonlinearity (NNL) index was purposed to

quantify and determine the influencing factors of the nonlinear interaction of storm surge under climate change conditions. This work served as a proof-of-concept to the dynamic modeling system and focused only on the Mississippi and Alabama coast, and included limited changes to the coastal landscape and sea level.

Passeri et al. [2015a] began to examine the potential changes to the shoreline position and profile under SLR along the Florida Panhandle coast. They extrapolated historic rates of shoreline change in conjunction with an equilibrium beach profile approach to estimate future shoreline positions under an intermediate SLR scenario for the year 2050. Using hydrodynamic simulations, they indicated that the simulated storm surge was highly sensitive to shoreline change, and back bays protected from barrier islands were highly vulnerable to increased storm surge because of additional barrier island overtopping. *Passeri et al.* [2016] continued this work with a focus on validating the modeling framework for astronomic tides and shoreline morphology. They used a high-resolution astronomic tide, wind-wave, and hurricane storm surge presented by *Bilskie et al.* [2015b] that contains the entire coast of Mississippi, Alabama, and the Florida Panhandle. The model's representation of the coastal landscape was modified based on an estimate of future shoreline positions and primary dune heights for four SLR derived from a Bayesian network purposed in *Plant et al.* [2016].

Based on the conclusions and recommendations of these previous studies, the natural progression is to develop a modeling system to estimate and investigate storm surge flooding under climate change conditions by taking into account three major landscape changes: (1) shoreline and barrier island morphology, (2) marsh evolution, and (3) LULC change. As stated in *Passeri et al.* [2015c], a large-scale, physics-based storm surge modeling framework that accounts for these changes and their interrelation with varying climate and SLR scenarios does not exist. To properly examine the additional flood risk and the vulnerability of coastal communities to extreme flooding in the future, these conditions must be incorporated into the computational modeling approach. The objective of this paper is to assess the state of the practice and provide a suggested physics-based storm surge modeling framework to simulate hurricane storm surge in a changing climate while considering changes to the coastal landscape. This work is a culmination of the research presented in *Bilskie et al.* [2014], *Passeri et al.* [2016], and *Plant et al.* [2016]. The developed methodology is applied across the coastal floodplain regions of Mississippi, Alabama, and the Florida Panhandle, henceforth, referred to as the northern Gulf of Mexico (NGOM).

2. Methods

2.1. Wave and Storm Surge Model

The tightly coupled SWAN + ADCIRC (Simulating Waves Nearshore + ADvanced CIRCulation) code was utilized to compute water surface elevations, depth-averaged velocities and wave radiation stresses [*Dietrich et al.*, 2011] for various hurricane events and climate change scenarios. The 5.5 million node *NGOM3* mesh was applied and spans the western north Atlantic tidal (WNAT) model domain with model resolution down to 20 m along the NGOM coast [*Bilskie et al.*, 2015b] The high model resolution was included to incorporate high topographic accuracy as well as provide high spatial resolution in the model result [*Bilskie and Hagen*, 2013; *Bilskie et al.*, 2015a]. A new feature added for this work was the inclusion of biomass-corrected topographic elevations within the lower Apalachicola River marsh system [*Medeiros et al.*, 2015]. The *NGOM3* mesh was developed to represent ca. 2012 conditions and has been extensively validated for Hurricanes Isaac (2012), Dennis (2005), Katrina (2005), and Ivan (2004) [*Bilskie et al.*, 2015b] (Figure 1). The *NGOM3* model was modified to

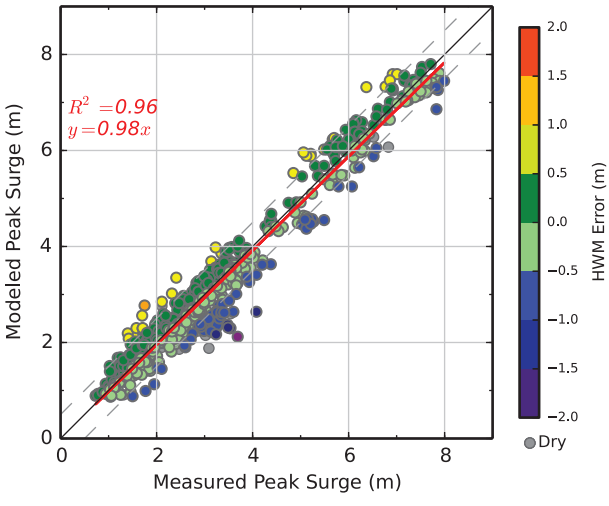

Figure 1. Comparison of measured and simulated peak surge for Hurricanes Ivan (2004), Dennis (2005), Katrina (2005), and Isaac (2012).

represent four global climate change scenarios for the year 2100, as presented in the following sections: Section 2.2 describes how SLR was incorporated into the model, Section 2.3 presents the methodology of incorporating shoreline and primary dune height change, Section 2.4 describes projections of the landscape roughness for the climate change scenarios, and Section 2.5 outlines the historical hurricanes used to force the suite of model configurations.

2.2. Incorporation of Sea Level Rise Into the *NGOM3* Model

Parris et al. [2012] established four SLR scenarios for the year 2100 of 0.2 m (low), 0.5 m (intermediate-low), 1.2 m (intermediate-high), and 2.0 m (high). The four SLR scenarios were incorporated in the SWAN + ADCIRC storm surge model setup; however, including SLR as a boundary condition in a tidal or storm surge model is not straightforward and can be accomplished using two general methods. The first method, the eustatic method, offsets the model's mean sea level by a given amount of SLR. Generally, this is applied by increasing the initial water level offset from the geoid. The eustatic method permits the direct application of appropriate projections of SLR as well as relative SLR. This method was used in the following studies: *Passeri et al.* [2015b], *Irish et al.* [2014], *Bilskie et al.* [2014], and *Atkinson et al.* [2013], to name a few. The second method, the boundary method, applies a zero-phase forcing function with an amplitude equal to a given SLR. The boundary method is applied at the open ocean boundary and allows the SLR to propagate through the domain as guided by the models' governing equations, much like a tidal forcing without periodicity. This method was used in *Bacopoulos and Hagen* [2014] and *Hagen and Bacopoulos* [2012].

Two simulations were performed for two SLR scenarios (intermediate-low and intermediate-high) to determine the appropriate method to include SLR. Both simulations utilized a coarse unstructured mesh of the WNAT model domain [*Hagen et al.*, 2006] and were forced with winds and pressure representative of Hurricane Katrina. The first two simulations employed the eustatic method. The second two simulations employed the boundary method. A 10.0-day spinup of a zero-phase tidal amplitude equal to the SLR was introduced prior to the Hurricane Katrina meteorological forcing. Differences in maximum storm surge between each type of SLR forcing for each of the SLR scenarios tested were minimal. Only minor differences (less than $\pm$5 cm) were observed. The boundary forcing method requires additional computational time because of the required spinup of the forcing along the boundary. Because of the minor differences in maximum storm surge and the additional computational time required for the boundary method, the eustatic method is used for all subsequent simulations.

2.3. Incorporation of Shoreline and Dune Height Evolution Into the *NGOM3* Model

Coastal morphology has the potential to alter hydrodynamic patterns; therefore, hydrodynamic assessments of SLR must consider concurrent changes to the shoreline [*Passeri et al.*, 2015c]. Because of the complex nature of coastal processes, modeling long-term morphodynamics is not a simple task. Historical data can be advantageous when analyzing the impacts of morphologic change on hydrodynamics. Hydrodynamic models can be modified with historic morphologic and sea level data to observe the impacts to astronomic tides and hurricane storm surge [*Bilskie et al.*, 2014; *Passeri et al.*, 2015b]. In addition, historic trends (e.g., historic shoreline change rates) can be extrapolated to obtain projections of future morphology for hydrodynamic assessments of SLR [*Passeri et al.*, 2015a]. However, historical trends do not account for changes that may occur under accelerated rates of SLR. Although process-based modeling can be used to simulate morphodynamic processes, long-term simulations tend to be inefficient and lengthy because of differences in hydrodynamic and morphologic time scales [*Dissanayake et al.*, 2012]. As a result, simulations are often restricted to small temporal and spatial scales [*Ding*, 2012]. On the contrary, probabilistic simulations of natural systems are beneficial because they can be implemented across large domains with relatively low computational expense. Bayesian Networks (BNs), based on the application of Bayes' theorem, evaluate the probability of a specific outcome based on relationships between input variables. For this study, the BN presented by *Plant et al.* [2016] was used to define relationships among various hydrodynamic drivers, geological constraints, and coastal responses to make probabilistic predictions of shoreline change and dune heights under various SLR scenarios along the Gulf of Mexico coastline.

For each of the four SLR scenarios, the BN was employed to project horizontal shoreline change and primary dune height at sampling locations along the NGOM (Figure 2a). The present day digital elevation model (DEM) was masked, from the 0 m NAVD88 contour to the local depth of closure, to generate polygon sections between the sampling locations. The masked polygon DEM sections were individually shifted

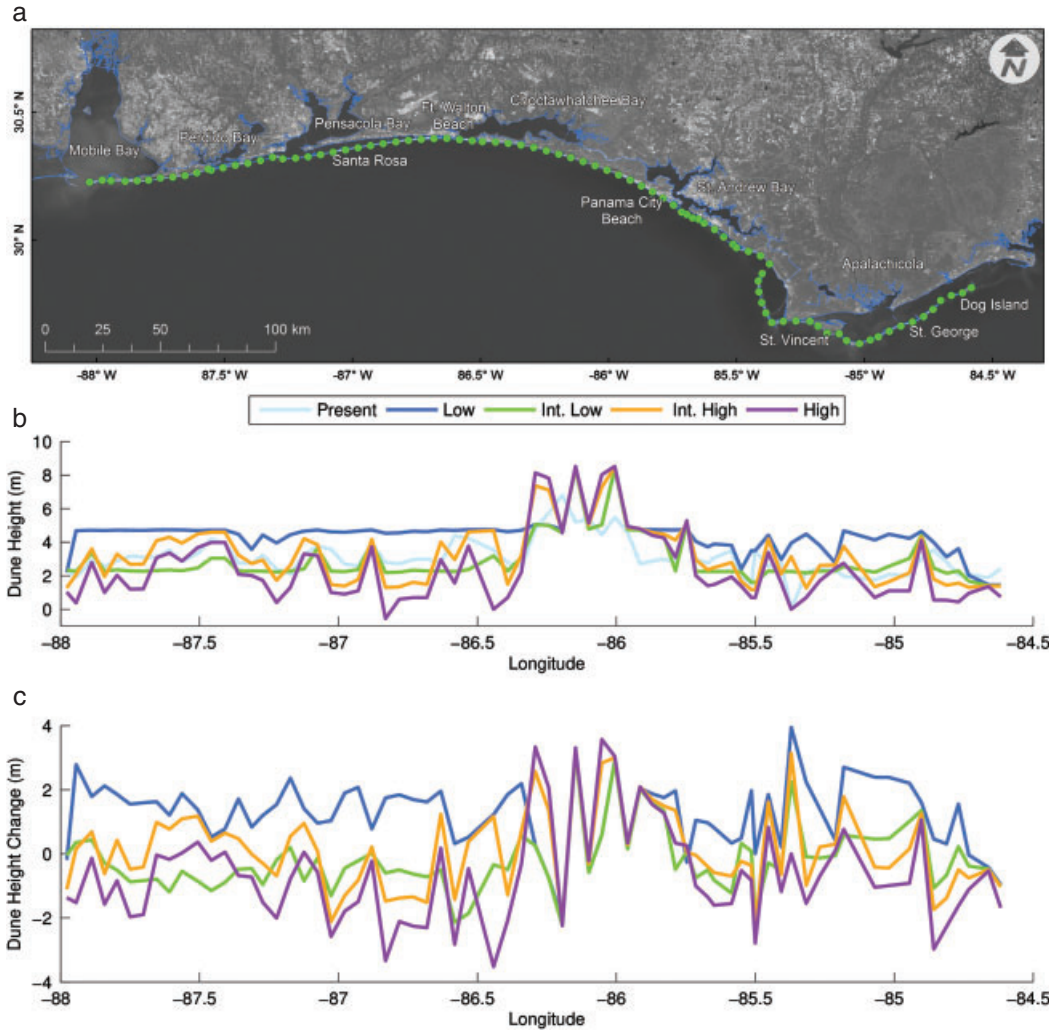

Figure 2. (a) Sampling locations for shoreline change and primary dune. (b) Primary dune heights for present day (ca. 2015) and projections for each sea level rise (SLR) scenario. (c) Change in dune height from present day for each SLR scenario. Negative change indicates a reduction in dune height. The basemap in (a) was provided by Esri.

landward (erosion) or seaward (accretion) according to the BN projection. In regions where the shoreline change was projected to exceed the infrastructure line, it was assumed that coastal defenses (e.g., nourishment, sea walls, etc.) will be put in place to stop the encroaching sea *Passeri et al.*, [2016]. In addition, the Mississippi-Alabama barrier island chain was modified to account for future westward lateral migration. The historic migration rates were used to extrapolate the total lateral growth for each island as well as their erosion along the eastern edge *Passeri et al.*, [2016].

In similar fashion, the primary dune heights were modified according to the BN network (Figures 2b and 2c) for each SLR scenario. The BN predicts that lower rates of SLR generally result in stable shorelines and higher dunes (greater than 2 m). The BN model also projects low dune heights (0.5 – 2.0 m) and increased shoreline erosion under high SLR *Plant et al.*, [2016]. The end results are four variations of the *NGOM3* model that incorporate shoreline change and changes to the primary dune height for each SLR scenario.

2.4. Nearshore Landscape Change and Intertidal Marsh Evolution

LULC datasets describe the physical land type and type of human use. For example, land cover distinguishes different types of forest or marsh vegetation and land use differentiates between residential, industrial, or agricultural lands. National, State, and local agencies produce LULC datasets for a variety of applications such as planning, stormwater basin characteristics, and habitat mapping. Hydrodynamic models make use

Table 1. Sea Level Rise (SLR) Scenarios Linked to Climate Change Scenarios for Land Use Land Cover Selection

SLR Scenario	SLR	Climate Change/Land Use Scenario
Present	0.0	B1
Low	0.2	B1
Intermediate-low	0.5	B1
Intermediate-high	1.2	A1B
High	2.0	A2

of LULC to prescribe surface roughness characteristics, namely bottom friction, surface canopy, and wind reduction factors [*Bunya et al.*, 2010; *Atkinson et al.*, 2011].

Bottom friction is often parametrized by spatially varying Manning's *n* coefficients that represent the resistance of flow for different land types [*Chow*, 1959]. Each type of LULC can be associated with a range of Manning's *n* values. Different LULC types can also reduce wind velocity in dense vegetation. Surface canopy coefficients can limit the momentum transfer from the wind to the water surface in dense vegetation such as in some marsh grasses and wetlands, mangroves, and forest. In addition, vertical obstacles, such as dense forest and buildings, can reduce wind velocity downwind.

The U.S. Geological Survey (USGS) Earth Resources Observation System Center (http://landcover-modeling.cr.usgs.gov/) has produced yearly LULC maps for future carbon emissions scenarios (B2, B1, A2, and A1B) up to the year 2100 for the continental U.S. [*Sleeter et al.*, 2012]. For all carbon emission scenarios, developed land is projected to increase at the expense of a reduction in forest and other natural land cover types. Changes to future LULC have a direct relationship with the surface roughness as previously described. The four SLR scenarios prescribed by *Parris et al.* [2012] were linked to a particular carbon emission scenario used to derive the surface roughness parameters from the USGS LULC maps for the year 2100 (Table 1). For example, the intermediate-high SLR scenario was associated with the A1B carbon emission scenario; therefore, the USGS A1B 2100 LULC map was employed to derive the surface roughness characteristics for the intermediate-high model configuration.

The USGS LULC projections do not consider potential transformations of the intertidal salt marsh from a rise in sea level. Salt marsh is sensitive to local tidal conditions and productive when its elevation resides between the local mean high water (MHW) and mean low water (MLW). If the rate of SLR increases too rapidly, the salt marsh will shift out of equilibrium and drown. The marsh may also migrate upland in new regions exposed to daily tidal flooding. In addition, lower rates of SLR may promote and sustain current marsh growth [*Morris et al.*, 2002; *Hagen et al.*, 2013; *Alizad et al.*, 2016].

A high-resolution hydrodynamic and biological model (HYDRO-MEM) of salt marsh productivity under SLR has established that land elevations lower than MLW become open water and land elevations that are between MHW and MLW provide ideal conditions for new salt marsh productivity [*Hagen et al.*, 2013; *Alizad et al.*, 2016]. General processes obtained from localized HYDRO-MEM modeling at specific locations along the NGOM were applied. For example, the evolution of salt marsh was considered via modifying Manning's *n* roughness coefficients for a given SLR scenario. Manning's *n* was assigned to open water if the location is hydraulically connected to the open ocean and its local elevation is less than MLW under SLR. Manning's *n* was assigned as new marsh (0.07) if the local elevation, under SLR, is between MLW and MHW and is not marsh under present conditions.

The resulting Manning's *n* bottom friction for each SLR scenario are shown in Figure 3. Bottom friction within the salt marsh regions (e.g., Apalachicola marsh, Mobile-Tensaw marsh, Grand Bay marsh, and Pascagoula marsh) decreased with increasing sea level. As the sea level rises, additional areas include elevations less than MLW indicating open water with a reduced bottom friction. New regions are exposed to daily flooding and their elevation is within mean sea level and MHW resulting in a reduction in bottom friction. This is observed by the increasing areas of light blue in Figure 3 around the low-lying regions. Furthermore, the projections of LULC drive reductions of bottom friction near the coastal cities. For example, Mobile, AL (located in northwest Mobile Bay) is projected to have an increase in population and thereby, land use is

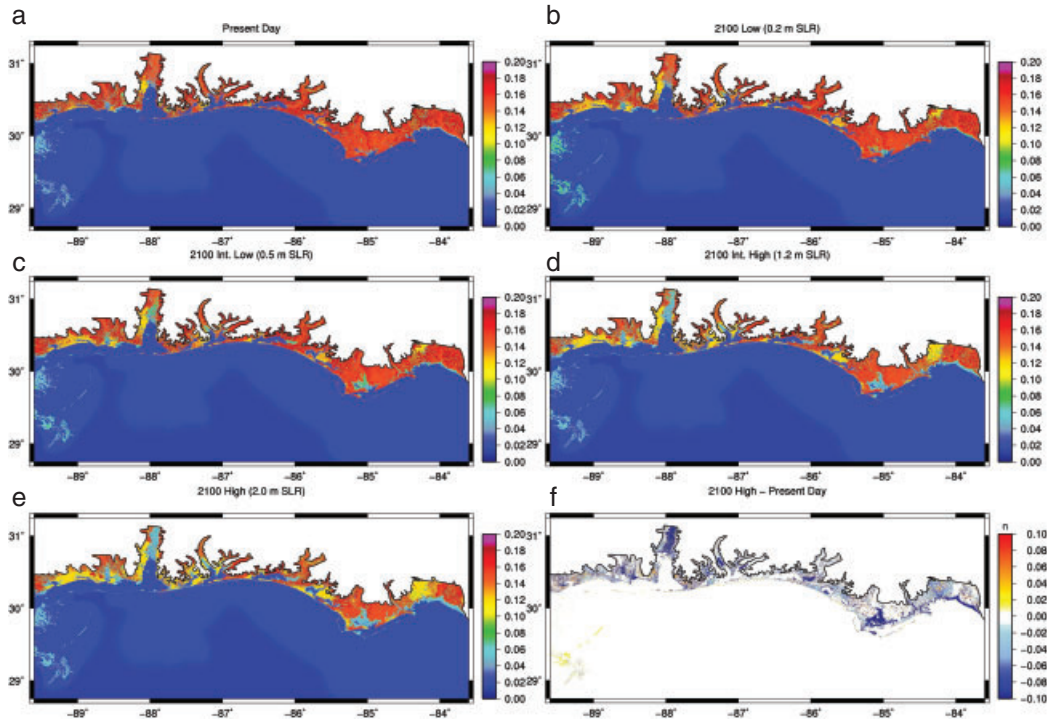

Figure 3. Manning's *n* bottom roughness across the northern Gulf of Mexico for (a) present day, (b) 2100 low (0.2 m SLR), (c) intermediate-low (0.5 m SLR), (d) intermediate-high (1.2 m SLR), (e) high (2.0 m SLR) SLR scenarios, and (f) difference in Manning's *n* between the 2100 high (e) and present day (a).

expected to change from largely forested lands to developed, reducing bottom friction. This is observed in the decrease of the warm colors to increasingly yellow in Mobile, AL and along the other coastal cities. Similar trends occur for the wind reduction factors.

2.5. Historic Hurricanes and Storm Selection

We examined records of hurricane wind and storm surge inundation to assess hurricane-generated storm surge potential related to climate change along the NGOM. We utilized SURGEDAT, a comprehensive storm surge database for the U.S. Gulf Coast [*Needham et al.*, 2015], to provide storm surge data. SURGEDAT has archived more than 5200 high water marks (HWM) from tropical cyclones (hurricanes and tropical storms) along the U.S. Gulf coast since 1880 [*Needham et al.*, 2013]. These data were compiled from more than 60 separate sources, including Federal Government sources, academic literature, and daily periodicals in the region [*Needham and Keim*, 2012]. SURGEDAT provides a useful history of our study area, as the database provides HWMs at Apalachicola generated from 33 unique tropical cyclones since 1880. The two highest water levels at this location reached 3.05 m from an unnamed hurricane in 1903 and Hurricane Elena in 1985. To depict the broader storm surge history along the NGOM, histograms were generated to show the recorded surge events ranked by magnitude across the NGOM region. The analysis resulted in 10 hurricane events that contributed to the majority of observed peak surges: Hurricanes Isaac (2012), Katrina (2005), Dennis (2005), Ivan (2004), Georges (2004), Earl (1998), Opal (1995), Kate (1985), Elena (1985), and Agnes (1972) (Figure 4).

2.6. Storm Surge Simulations

A total of 60 SWAN + ADCIRC simulations were performed. The model was forced using meteorological wind and pressure fields for each of the 10 hurricane events developed from a composite of objectively analyzed observations and modeled winds and pressures [*Cox et al.*, 1995; *Powell et al.*, 1998; *Bunya et al.*, 2010]. The 10 hurricane events forced each of the five model configurations: present day, 2100 low, intermediate-low, intermediate-high, and high. In addition, all 10 storms were forced using the present day model configuration but only include the intermediate-high SLR scenario (1.2 m); this experiment was designed to assess

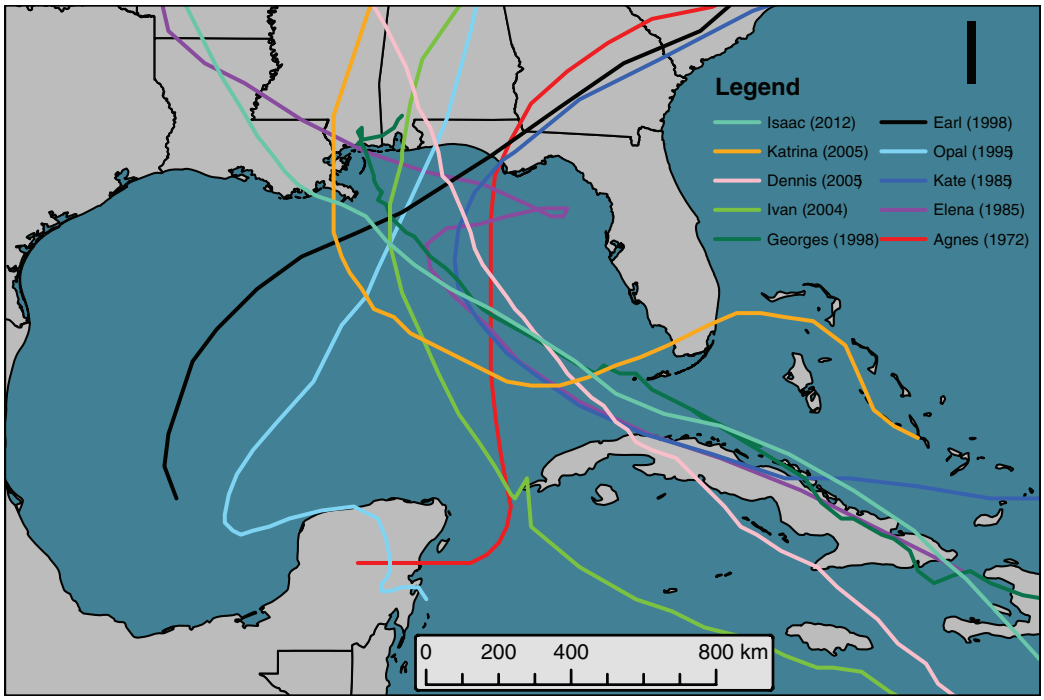

Figure 4. Historical hurricane tracks. Hurricane track data obtained from weather.unisys.com.

the maximum storm surge response to the landscape changes. From the suite of simulations, a maximum of maximums (MOMs) surface was derived for each SLR scenario as forced by the 10 historic hurricanes resulting in five MOM surfaces, as well as a MOM surface for the intermediate-high SLR with no landscape change experiment. The MOM was computed by recording the maximum simulated water surface elevation at each computational node from the maximum value obtained in each of the 10 simulations for each SLR scenario.

3. Results

3.1. Simulated Maximum Storm Surge

The simulated MOM storm surge for the present condition and four SLR scenarios along the Mississippi, Alabama, and Florida coast are shown in Figure 5. Under present conditions, a maximum simulated storm surge of 7–8 m occurred along the Mississippi coast (Figure 5a), contributed by Hurricane Katrina. Along the eastern Alabama coast and Florida Panhandle, the maximum storm surge was 2–3 m. Within the bay systems, such as Mobile, Pensacola, and Apalachee Bay, the storm surge was generally 3–4 m. These bays have sufficient fetch lengths for locally generated surges to increase water levels. Choctawhatchee Bay, the most enclosed bay in the region, experienced the lowest surge values of 1–2 m.

The simulated MOM for the low, intermediate-low, intermediate-high, and high condition are shown in Figures 5b–5e, respectively. Trends in the locations of the maximum simulated surge were similar to the present scenario (Figure 5a). Coastal Mississippi experienced the highest surge levels for all scenarios and increased surge was observed in northern Mobile Bay, northern Pensacola Bay, and Apalachee Bay. Under the high SLR scenario, surge levels in Choctawhatchee Bay increased to 4–5 m and were similar to those along the Gulf coast. The drastic increase within Choctawhatchee Bay was caused by the reduction in the primary dune height by ~3 m near the inlet for the high scenario (Figure 2), which allowed local overtopping and increased surge in the bay. In addition, the effective fetch within the bay increased resulting in increased surge. The higher SLR scenarios (intermediate-high and high) drastically reduced dune heights in addition to increased erosion. The landward penetration of the shoreline, lower primary dune heights, and a higher sea level enabled increased inundation along the NGOM barrier islands and increased surge levels within the bays.

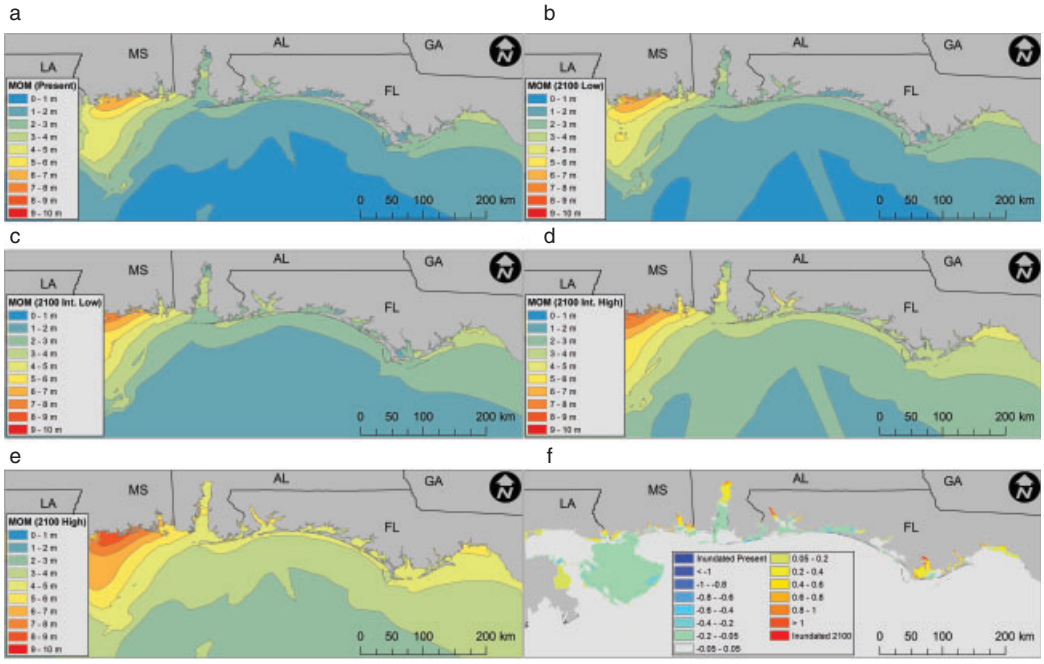

Figure 5. Simulated maximum of maximums (MOMs) storm surge (a) under present conditions [0 m sea level rise (SLR)], (b) 2100 low (0.2 m), (c) 2100 intermediate-low (0.5 m), (d) 2100 intermediate-high (1.2 m), (e) 2100 high (2.0 m) SLR scenarios, and (f) difference between the model simulations of with and without landscape changes for the intermediate-high scenario.

To quantify the increase in flooding, the total inundated land area was computed for each MOM along the Mississippi, Alabama, and Florida Panhandle coast (Table 2). The total inundation increased for each scenario beginning with 2986.5 km^2 for the present condition to 5581.6 km^2 for the high scenario, a change of 87%. The largest increase in inundation area, 27%, was from the intermediate-low (3584.2 km^2) to the intermediate-high (4557.9 km^2) scenario. The inundated area was computed for developed and agricultural (farm and pasture) land use classifications using the 2011 National Land Cover Database (NLCD). The 2011 NLCD data were used for all scenarios to apply a consistent dataset for the computation of inundated land, rather than using each scenario's respective LULC map. Under present conditions, the MOM inundated 282.7 km^2 of developed land, and under the high scenario 672.3 km^2, an increase of 138%. Similar to the total inundated land area, the largest percent change of 35% was found between the intermediate-low (375.4 km^2) and intermediate-high scenario (506.4 km^2). The increase of 131 km^2 was larger than the land area of many of the coastal cities along the NGOM, which generally have land areas from 50 to 100 km^2. This trend continues when examining the additional flooding across agricultural land. Under present day conditions, the total inundated agricultural land was 11.3 km^2, but increased to 32.6 km^2 under the high scenario, a percent change increase of 189%. The most drastic increase, however, was between the intermediate-low and intermediate-high scenario, which inundated 15.7 and 24.2 km^2 of agricultural land, respectively. According to the USDA, the average cost of farm real estate in 2014 across Mississippi, Alabama, and Florida was $860,666 per km^2 (www.usda.gov). Although the magnitude in agricultural inundation was relatively small, the increase in flood risk could potentially result in hundreds of millions of dollars in damages, up to ~$280 million for the high scenario in 2014 dollars.

3.2. Impact of Landscape Change on Simulated Maximum Storm Surge

The MOM from simulating all 10 hurricanes using the present day model with the intermediate-high scenario subtracted from the MOM that considered the 2100 intermediate-high landscape change and SLR (Figure 5d) is shown in Figure 5f. The gray regions indicate no change occurred; in other words, incorporating landscape changes did not alter the maximum simulated storm surge. Most of the offshore regions suggest that no change occurred with the exception of minor differences of −0.07 m offshore of southwestern Mississippi. In general, the MOM-derived without landscape change produced higher surge values from

Table 2. Total Inundated Land Area (km^2) and the Inundated Area for Developed and Agriculture Land Use for Each Scenario.

	Inundated Area (km^2)		
Sea Level Rise Scenario	Total	Developed	Agriculture
Present	2986.5	282.7	11.3
Low	3132.5	301.8	12.3
Intermediate-low	3584.2	375.4	15.7
Intermediate-high	4557.9	506.4	24.2
High	5581.6	672.3	32.6

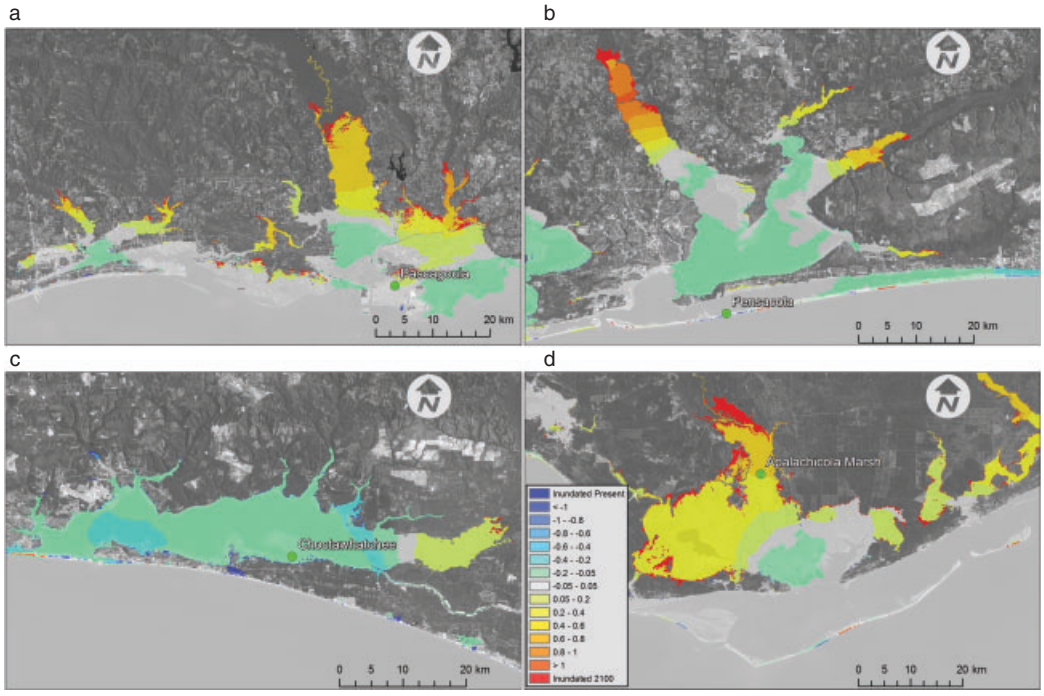

Figure 6. Insets as shown in Figure 5f for (a) Biloxi Bay and Pascagoula, (b) Pensacola Bay, (c) Choctawhatchee Bay, and (d) Apalachicola. The basemap was provided by Esri.

0.05 to 0.2 m compared with the MOM that included the landscape changes. However, along the inundation extent, the model simulation with landscape change produced larger maximum surge.

Closer inspection of the differences in maximum storm surge with and without 2100 intermediate-high landscape changes are shown for Biloxi Bay and Pascagoula (Figure 6a), Pensacola Bay (Figure 6b), Choctawhatchee Bay (Figure 6c), and Apalachicola (Figure 6d). Within Biloxi Bay, Pascagoula, and Grand Bay regions, there were minor differences between the MOMs (Figure 6a). The variances were more drastic along the inundation extents; however, the furthest reaches of the flood extent showed that the simulation with landscape change produced 0.5–0.70 m higher surge. In addition, as indicated in Figure 6a, new regions were exposed to flooding when using the landscape change model. The model simulation that only incorporated the 2100 intermediate-high SLR scenario, and not the associated landscape changes, under-predicts the flooding extent, and in most areas of maximum surge.

Model results in Pensacola Bay (Figure 6b), Choctawhatchee Bay (Figure 6c), and Apalachicola (Figure 6d) produced similar results; however, there were large differences in maximum storm surge along the barrier islands. Differences of $\pm$0.80 m existed along Santa Rosa Island and $\pm$1 m near Choctawhatchee Inlet. The Apalachicola barrier island chain (St. Vincent, St. George, and Dog Islands) included stretches of land that were overtopped when incorporating the landscape change, namely the reduction in primary dune height

and regions that were not flooded using the future projections. The results along the barrier islands indicate the importance of incorporating dune height morphology. Within the interior of the bays, there were small differences of −0.05 to −0.20 m, similar to those found in Biloxi Bay, Pascagoula, and Grand Bay (Figure 6a). Simulated maximum storm surge was increased under the landscape change scenario at the head of each bay. The low-lying regions near the coastal rivers were susceptible to additional inundation, specifically in northwestern Pensacola Bay and in the marsh north of Apalachicola Bay. The reduction in the primary dune height and reduced bottom roughness for the intermediate-high scenario promoted an increased storm surge height from 0.20 to 1 m and an increase in total inundation area. In the Pascagoula and Apalachicola marsh, the reduction in bottom friction resulted in up to 0.50 m of increased water level as well as additional flooding. The reduction in the bottom friction induced by the evolution of the salt marsh reduced the surge attenuation. Not accounting for such changes to bottom friction in the marsh regions may cause a substantial under-prediction in maximum water levels.

3.3. Nonlinearity of Storm Surge Under SLR

From the MOM, it is difficult to ascertain the additional water level induced by SLR. To assess the increase in the simulated maximum storm surge for each SLR scenario, we utilize the NNL index from [*Bilskie et al.*, 2014]:

$$\mathrm{NNL}\ (x,y) = \frac{\eta\,(x,y)_{\mathrm{SLR}} - \eta\,(x,y)_{\mathrm{base}}}{\lambda} - 1 \tag{1}$$

where $\eta(x,y)_{\mathrm{SLR}}$ is the dynamically simulated maximum water surface elevation for a given SLR scenario at x,y, $\eta(x,y)_{\mathrm{base}}$ is the simulated maximum water surface elevation for a base condition (present condition), and λ is the amount of SLR. Locations where NNL equals zero indicate that maximum storm surge increased linearly by the amount of SLR ($\eta_{\mathrm{SLR}} = \eta_{\mathrm{present}} + \lambda$). Locations where NNL is larger than zero indicate that surge is greater than the amount of SLR and a value less than zero indicates that maximum surge is less than the amount of SLR.

The NNL values were computed for each SLR scenario (with the present condition as the base scenario) and are shown in Figure 5. Gray areas indicate maximum surge increased linearly by the amount of SLR, warm colors indicate an amplification (maximum storm surge increased by more than the applied SLR), purple shows regions wetted under SLR and not under present day conditions, and cool colors suggest de-amplification with respect to the amount of SLR (the difference in maximum storm surge from present day was less than the applied SLR). Because of the relatively deep water and low bottom friction, the increase in maximum storm surge offshore is largely equal to the amount of SLR, and it is evident, within the nearshore region, the storm surge response to SLR for this coastal area is nonlinear.

The NNL from the low scenario (compared to the present) (Figure 7a) suggested a linear rise in maximum storm surge offshore. There is little change in regions where the water surface and velocity gradients were relatively smooth, such as in the deeper waters. Approaching shallower water and the complex coastline of the NGOM causes the surge response under SLR to become nonlinear. Within the bay systems, such as Mississippi Sound, the Bay of St. Louis, Biloxi Bay, Grand Bay, Mobile Bay, Pensacola Bay, and Apalachicola Bay, the surge response was generally reduced relative to the low SLR of 0.2 m; Choctawhatchee Bay indicated a linear rise in surge. Maximum surge was increased by less than the applied SLR as new areas were exposed to inundation, thereby decreasing water levels on the backside of the new flooding. The additional SLR allowed water to penetrate farther inland. This was further illustrated by the high NNL values at the flooding extents, namely near Pascagoula, north Mobile Bay, Pensacola Bay, and in Apalachicola. With the present day sea level, these regions experienced low flood inundation depths; under low SLR, flood depths in these regions increased (see orange and red areas in Figure 7a). In addition, land (and wind) shielding effects also caused negative values of NNL, such as observed on the backside of the Chandeleur Islands, Mississippi Barrier Islands, and the Apalachicola Bay barrier islands.

Increasing the sea level from 0.2 to 0.5 m (intermediate-low), in addition to the respective landscape changes, results in a spatially different pattern of NNL values (Figure 7b). Offshore, NNL values were still zero and were expected to be consistent for all SLR scenarios, but the bays showed positive values of NNL. Within Mississippi Sound, Biloxi Bay, Grand Bay, and Apalachee Bay NNL values remained negative. These bays are not protected as those located along the Florida Panhandle coast. The bays along the Florida Panhandle are sheltered and include narrow inlets. The intermediate-low SLR scenario results in a reduction

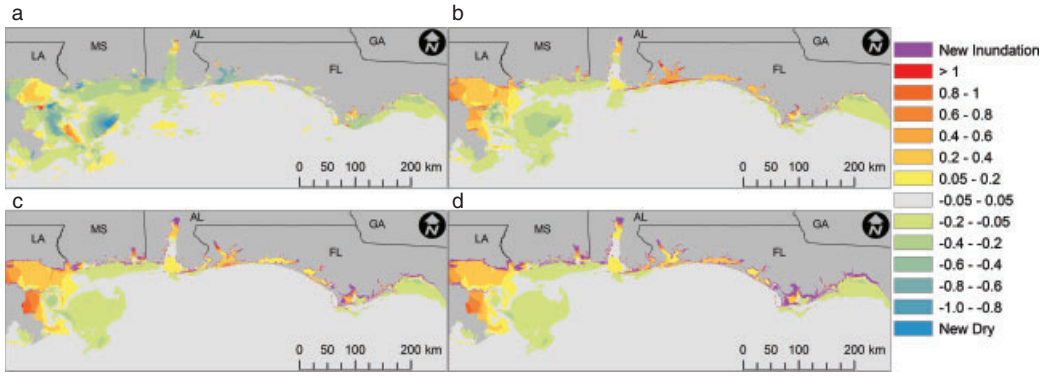

Figure 7. Normalized nonlinearity index from the maximum of maximums (MOMs) for the (a) low, (b) intermediate-low, (c) intermediate-high, and (d) high sea level rise scenario, relative to the present day MOM.

of dune heights along the barrier islands (Figure 2) and increased shoreline erosion. This coupled with a SLR of 0.5 m yields additional storm surge overtopping across the barrier islands, resulting in additional surge within the bay systems. High NNL values of 1.3 were observed within Santa Rosa Sound suggesting local surge increase by 1.15 m ($\Delta\eta = \lambda(1 + \mathrm{NNL})$). Similarly, NNL values of 1.3–1.5 were computed at the inundation extent of Pensacola Bay. Generally, high NNL values were observed along the edge of the new inundation areas, as also observed for the low scenario (Figure 7b).

The NNL patterns for the intermediate-high scenario (1.2 m SLR) were similar to the intermediate-low scenario (0.5 m SLR); however, the magnitudes were reduced (Figure 7c). Within Mississippi Sound, Grand Bay, and Apalachee Bay, the area of negative NNL values decreased in size compared with the intermediate-low scenario. The NNL values in the Florida Panhandle bay systems were still greater than one, but less than those NNL values observed for the intermediate-low. Generally, the dune heights were further reduced, and with an increased sea level most regions trended toward an open coast behavior (i.e., linear response). In addition, similar trends of large NNL values were found adjacent to regions of new inundation. The nonlinear response was evident in the land adjacent to Pascagoula, MS, specifically near U.S. 90. NNL values were negative on the south side of the highway and positive on the north side. Storm surge was increased under SLR and continued to overtop the highway increasing the relative flood depths on the north side of the road and not on the south side, with respect to the additional SLR. This phenomenon would not have been captured using a bathtub type SLR model as it does not consider physical mechanisms of the dynamics of storm surge and SLR, which go beyond the hydrodynamics and include the dynamics of shoreline and dune morphology, marsh evolution, and LULC change that are directly linked to the applied SLR scenarios.

The trend of NNL values approaching zero continues for most regions under the high SLR scenario (2.0 m) (Figure 7d). The exception is within Perdido and Choctawhatchee Bay. Perdido and Choctawhatchee, under present conditions, have narrow inlets and are protected by relatively high dune heights along the barrier islands. In addition, the increase in sea level allows water to flow between Mobile Bay and Perdido Bay, increasing the amount of potential surge volume into Perdido Bay and the surrounding floodplain. Similarly, under the high scenario, Santa Rosa Sound swells from increased inundation and allows water to flow from the Sound into Choctawhatchee Bay increasing surge levels. The NNL increased, from the intermediate-high scenario, because the enlarged exposure to the bays are not directly connected to the open ocean, but connected to Mobile Bay and Santa Rosa Sound. The regions that have increased exposure directly connected to the open ocean, such as Mobile Bay, Pensacola Bay, St. Andrew Bay, and Apalachicola Bay, tend to have NNL values reduced as they behave more like the open ocean (i.e., linear response to SLR).

3.4. Water Surface Elevation Time Series Under SLR

Thus far, we have only examined the peak storm surge under various SLR scenarios as well as the effect of landscape changes using the intermediate-high scenario as an example. A critical aspect to consider is the evolution of the storm surge in time, which is a characteristic only, a dynamic modeling framework allows for and is often overlooked. Time series of water surface elevations at four locations (shown in Figure 6) near Pascagoula, Pensacola, Choctawhatchee, and Apalachicola were obtained from the storm that produced the highest maximum storm surge for each location (Figure 8). The water surface elevations for each SLR

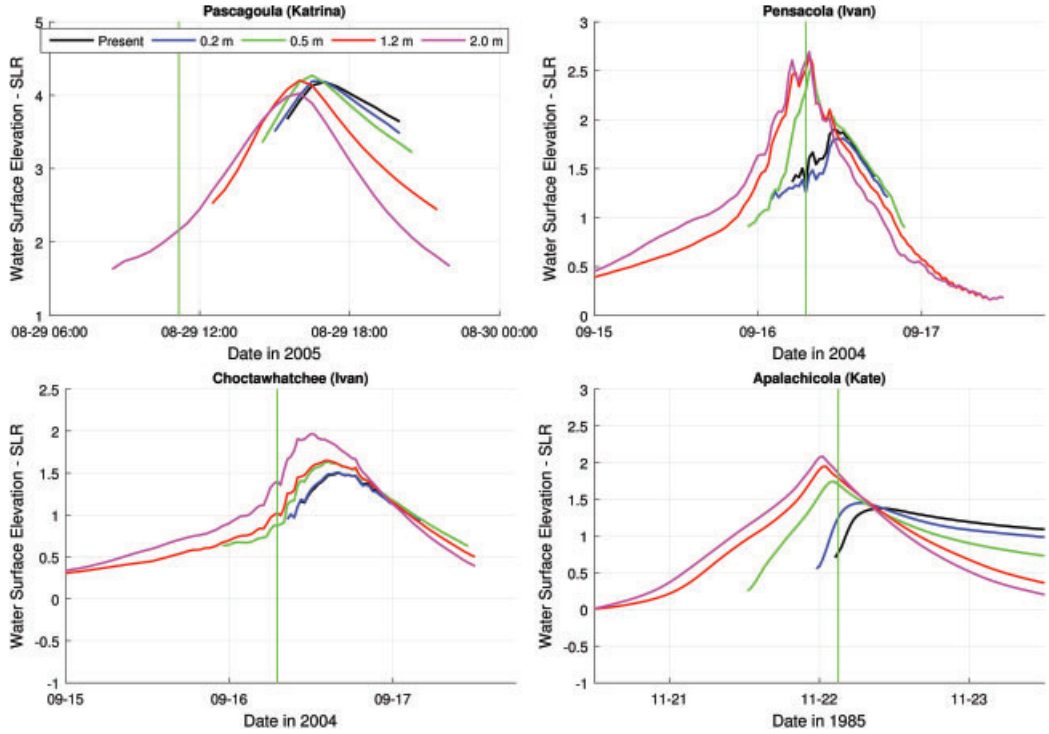

Figure 8. Time-series water surface elevation (m) hydrographs at Pascagoula during Katrina, Pensacola and Choctawhatchee during Ivan, and Apalachicola during Kate for present day. Locations are shown in Figure 6. Hydrographs shown for each sea level rise (SLR) are represented as the respective SLR subtracted from the simulated water surface elevation.

scenario were subtracted by the applied SLR. Three major results were obtained. First, at all four locations for all scenarios, none of the water surface elevations match the present day hydrograph indicating a dynamic response imposed by the SLR as well as the landscape changes. Second, an increase in sea level results in an increase in total inundation time. Third, the larger the SLR the earlier the peak surge occurs (Figure 8).

Although mild, the peak surge at Pascagoula increased beyond the applied SLR for the low and intermediate-low scenario but was reduced for the high scenario. However, the time of inundation doubled from ~5 h under present conditions to ~13 h for the high scenario. At the Pascagoula station, the peak surge for the low scenario was reduced with respect to the amount of SLR and for the intermediate-high and high scenario increased by over 0.5 m in addition to the SLR. At the time of landfall, the difference in peak surge between the low and high scenarios were greater than 1 m in addition to the SLR. At the Choctawhatchee location, the surge increases for each scenario up to an additional 0.5 m above the high SLR scenario along with an earlier arrival of the peak surge by several hours. At Apalachicola, the peak surge also arrived several hours prior as the sea level increased and an increase in sea level further amplified the peak surge, in addition to the SLR, by as much as 0.25 m for the intermediate-low and 0.5 m for the high scenario.

4. Discussion and Implications

This research supports the changing paradigm in the methods that coastal engineers and scientists employ to model the effects of climate change, and SLR in particular, on tidal and hurricane storm surge flooding [*Bilskie et al.*, 2014; *Orton et al.*, 2015; *Alizad et al.*, 2016; *Passeri et al.*, 2016]. State-of-the-art numerical tide and storm surge models are becoming resolved enough to capture the flood extent in fine detail [*Bilskie et al.*, 2015a]. With this, it is possible to alter these models with future projections of potential landscape change to assess the impacts of global climate change and SLR on coastal flooding. Assessments using static, or bathtub (i.e., drowned valley), inundation models have been found to over- or under-predict maximum storm surge-driven water levels and total inundation extent, especially in the nearshore and across the costal floodplain [*Zhang et al.*, 2013]. Static flood inundation models, although computationally inexpensive, do not account for physical processes such as wind-driven setup and bottom friction as well as the

time component, which is necessary to compute time of peak surge and total inundation time. Static models are also limited in their capacity to include landscape changes. Therefore, a dynamic model framework is necessary to evaluate storm surges under SLR.

Developed maximum storm surge flood inundation and MOM maps for each SLR scenario (Figure 5) show the change in storm surge height and the modified spatial distribution pattern of the flooding. This is attributed not only to the complex interaction between SLR and storm surge but also to changes in the landscape as incorporated into the model. This was demonstrated through the examination of the impact of landscape change on the simulated storm surge. The reduction in dune heights, in addition to SLR, increased barrier island overtopping and resulted in additional flood volume within many of the bay systems. The increased volume resulted in additional inundation along the banks of the bay and a significant increase in maximum water levels as high as ± 1 m across the low-lying regions at the head of each bay. The increased water level and additional inundated area also contributed to a reduction in bottom friction, whereby low-lying regions under SLR tend to mimic intertidal or open water conditions. The maps of NNL values show the large spatial variation of the storm surge response to SLR-driven landscape change (Figure 7). The pattern changes for each scenario, but general trends depict that flooding for most of the coastal floodplain is amplified and maximum storm surge will increase by more than the applied SLR.

These findings have a variety of implications and can provide a breadth of information for various coastal assessments of SLR. First, this work directly presents a methodology by which a present day tide and storm surge model can be adapted to examine coastal flooding under climate change. It provides evidence that local landscape changes can be accounted for in a large-domain modeling approach and the methodology can be translated to other low-gradient coastal landscapes. From a coastal management perspective, this model framework can be adapted to include engineered structures, beach nourishment, and natural and nature-based features (NNBFs) [*Bridges et al.*, 2015]. Varying configurations of NNBFs can be incorporated to evaluate their effectiveness at the local and regional level. This is especially useful not just for the nearshore regions, but across agricultural lands where the inundation time from hurricane-driven saltwater intrusion can impact the future harvest of crop or livestock. The storm surge model results can provide boundary conditions for local hydrodynamic and morphological models. These local models can span a single barrier island, for example, and compute sediment transport because of storm-induced barrier island overwash. They can also be used to evaluate salinity or sediment transport within individual bay systems during hurricane events [*Huang et al.*, 2014]. The local models can also evaluate the performance of current or planned infrastructure (bridge decks and pilings, offshore oil platforms, etc.) under climate change conditions. From a biologic or ecologic standpoint, the storm surge results can support assessments of habitat loss and the vulnerability of coastal wildlife species. Increased inundation from storm surges can alter shorelines, erode dune systems, affect salt marsh dynamics, and modify sediment and salinity patterns. This can directly influence the fate and population of sea turtles, beach mice, oysters, shrimp, and fish, for example [*Pike and Stiner*, 2007; *Reece et al.*, 2013; *Chen et al.*, 2014; *Solomon et al.*, 2014; *Huang et al.*, 2015].

Combined, the presented methodology, its application, and results offer various assessments that support coastal resource managers in their decision-making process. As supported by the methodology, coastal resources managers are provided a variety of scientifically defensible datasets based on plausible scenarios of climate change and SLR.

5. Conclusions

This research proposes a dynamic modeling framework to examine the effects of global climate change, and SLR in particular, on tropical cyclone-driven storm surge. The developed methodology is applied with a focus on the NGOM, specifically along the coastal regions of Mississippi, Alabama, and the Florida Panhandle. A large-domain tide, wind-wave, and hurricane storm surge model representing present conditions was modified to characterize the potential outlook of the coastal landscape under four SLR scenarios for the year 2100. The modifications encompassed shoreline and barrier island morphology, marsh migration, and LULC change. In addition, the method by which SLR is applied to a hydrodynamic model was evaluated. Shoreline morphology, including primary dune height, was acquired from a Bayesian Network model. The projection of salt marsh evolution was assimilated based on localized hydrodynamic-ecological models. Projections of LULC for varying carbon emissions scenarios were linked to the four SLR scenarios and guided changes

to the model via landscape roughness. For an increase in sea level, coastal cities broadened resulting in a reduction of forest and natural land cover types.

To test the methodology of including projected landscape changes in a hydrodynamic model, 10 historic hurricane events were simulated for each SLR scenario and the spatial and temporal variation of storm surge-induced water levels were examined. Between the present day and high scenario, the inundated land area increased by 87%. Among the developed land, inundation increased by 138%, and by 189% for agricultural land. This may lead to hundreds of millions of dollars in damages from hurricane- and SLR-induced saltwater intrusion across farmlands. Under the intermediate-high SLR scenario, it was shown that the inclusion of landscape changes can have a profound effect of maximum storm surge, especially in regions protected by barrier islands. High rates of SLR result in a reduction of dune height, which enhanced barrier island overtopping, and increased surge heights by as much as 1 m. The NNL was computed among all scenarios and large spatial variations in the amplification of storm surge were observed, with some regions subjected to an increase in maximum water level by as much as double the applied SLR. The analysis of the time series of water levels supports that the interaction of SLR and storm surge is nonlinear not only spatially but also in time, and an increase in sea level resulted in increased inundation time and an earlier arrival of the peak surge. These factors cannot be assessed using static modeling approaches.

Overall, the presented research advances the knowledge and understanding of the effects of climate change, and SLR in particular, on tropical cyclone-driven storm surge. The study also promotes the paradigm shift in using a dynamic modeling framework to account for potential changes to the landscape and provides a methodology for which to do so. The modeling approach presented goes beyond the hydrodynamics and includes the dynamics of shoreline and dune morphology, marsh evolution, and LULC change that are directly linked to the applied SLR scenarios. The results of this study have broad implications and can support localized hydrodynamic, morphologic, biological, and ecological assessments. The outcomes of this research ultimately provide a holistic understanding of the coastal system and aid in restoration and long-term coastal sustainability. This is achieved through improved tools for coastal resource managers to make informed decisions for the NGOM system and other coastal regions with similar characteristics.

References

Ablain, M., A. Cazenave, G. Valladeau, and S. Guinehut (2009), A new assessment of the error budget of global mean sea level rate estimated by satellite altimetry over 1993–2008, *Ocean Sci.*, *5*, 193–201, doi:10.5194/os-5-193-2009.

Ali, A. (1999), Climate change impacts and adaptation assessment in Bangladesh, *Clim. Res.*, *12*(2–3), 109–116, doi:10.3354/cr012109.

Alizad, K., S. C. Hagen, J. T. Morris, P. Bacopoulos, M. V. Bilskie, J. F. Weishampel, and S. C. Medeiros (2016), A coupled, two-dimensional hydrodynamic-marsh model with biological feedback, *Ecol. Modell.*, *327*, 29–43, doi:10.1016/j.ecolmodel.2016.01.013.

Atkinson, J. H., H. J. Roberts, S. C. Hagen, S. Zou, P. Bacopoulos, S. C. Medeiros, J. F. Weishampel, and Z. Cobell (2011), Deriving frictional parameters and performing historical validation for an ADCIRC storm surge model of the Florida Gulf Coast, *Fla. Watershed J.*, *4*(2), 22–27.

Atkinson, J. H., J. M. Smith, and C. Bender (2013), Sea-level rise effects on storm surge and nearshore waves on the Texas coast: influence of landscape and storm characteristics, *J. Waterw. Port Coastal Ocean Eng.*, *139*(2), 98–117, doi:10.1061/(asce)ww.1943-5460.0000187.

Bacopoulos, P., and S. C. Hagen (2014), Dynamic considerations of sea-level rise with respect to water levels and flooding in Apalachicola Bay, *J. Coastal Res.*, 43–48.

Bernier, N. B., K. R. Thompson, J. Ou, and H. Ritchie (2007), Mapping the return periods of extreme sea levels: allowing for short sea level records, seasonality, and climate change, *Global Planet. Change*, *57*(1–2), 139–150, doi:10.1016/j.gloplacha.2006.11.027.

Bilskie, M. V., and S. C. Hagen (2013), Topographic accuracy assessment of bare earth lidar-derived unstructured meshes, *Adv. Water Resour.*, *52*, 165–177, doi:10.1016/j.advwatres.2012.09.003.

Bilskie, M. V., S. C. Hagen, S. C. Medeiros, and D. L. Passeri (2014), Dynamics of sea level rise and coastal flooding on a changing landscape, *Geophys. Res. Lett.*, *41*(3), 927–934, doi:10.1002/2013GL058759.

Bilskie, M. V., D. Coggin, S. C. Hagen, and S. C. Medeiros (2015a), Terrain-driven unstructured mesh development through semi-automatic vertical feature extraction, *Adv. Water Resour. A*, *86*, 102–118, doi:10.1016/j.advwatres.2015.09.020.

Bilskie, M. V., S. C. Hagen, S. C. Medeiros, A. T. Cox, M. Salisbury, and D. Coggin (2015b), Data and numerical analysis of astronomic tides, wind-waves, and hurricane storm surge along the northern Gulf of Mexico, *J. Geophys. Res.*, doi:10.1002/2015JC011400.

Bridges, T. S., et al. (2015), Use of natural and nature-based features (NNBF) for coastal resilience, *Rep. SR-15-1*, U.S. Army Corps of Eng., Alexandria, Va.

Bunya, S., et al. (2010), A high-resolution coupled riverine flow, tide, wind, wind wave, and storm surge model for southeastern Louisiana and Mississippi. Part I: Model development and validation, *Mon. Weather Rev.*, *128*, 345–377, doi:10.1175/2009MWR2906.1.

Cazenave, A., and G. L. Cozannet (2014), Sea level rise and its coastal impacts, *'Earths Future*, *2*(2), 15–34, doi:10.1002/2013EF000188.

Chen, Q., H. Wang, L. Wang, R. Tawes, and D. Rollman (2014), Predicting impacts of tropical cyclones and sea-level rise on beach mouse habitat, *J. Coastal Res.*, 12–19.

Chow, V. T. (1959), *Open-Channel Hydraulics*, McGraw-Hill, New York.

Church, J. A., and N. J. White (2006), A 20th century acceleration in global sea-level rise, *Geophys. Res. Lett.*, *33*(1), L01602, doi:10.1029/2005GL024826.

Acknowledgments

This research was funded in part under award NA10NOS4780146 from the National Oceanic and Atmospheric Administration (NOAA) Center for Sponsored Coastal Ocean Research (CSCOR), award NFWMD-08-073 from the Northwest Florida Water Management District (NWFWMD), and the Louisiana Sea Grant Laborde Chair. This work used the Extreme Science and Engineering Discovery Environment (XSEDE), which is supported by the National Science Foundation (NSF) grant ACI-1053575 [*Towns et al.*, 2014]. This work also used High Performance Computing at Louisiana State University (LSU) and the Louisiana Optical Network Initiative (LONI). The statements and conclusions are those of the authors and do not necessarily reflect the views of NOAA, NWFWMD, Louisiana Sea Grant, XSEDE, NSF, LSU, or LONI. All data for this paper are properly cited and referred to in the reference list. Any use of trade, firm, or product names is for descriptive purposes only and does not imply endorsement by the U.S. Government.

Cox, A. T., J. A. Greenwood, V. J. Cardone, and V. R. Swail (Eds) (1995), *An Interactive Objective Kinematic Analysis System*, Alberta, Canada.
Dietrich, J. C., M. Zijlema, J. J. Westerink, L. H. Holthuijsen, C. N. Dawson, R. A. Luettich, R. E. Jensen, J. M. Smith, G. S. Stelling, and G. W. Stone (2011), Modeling hurricane waves and storm surge using integrally-coupled, scalable computations, *Coastal Eng.*, *58*, 45–65, doi:10.1016/j.coastaleng.2010.08.001.
Ding, Y. (2012), Sea-level rise and hazardous storms: impacts on coasts and estuaries, in *Handbook of Climate Change Mitigation*, edited by W. Y. Chen, J. Seiner, T. Suzuki, and M. Lackner, Springer Science + Business Media, LLC.
Ding, Y., S. Nath Kuiry, M. Elgohry, Y. Jia, M. S. Altinakar, and K.-C. Yeh (2013), Impact assessment of sea-level rise and hazardous storms on coasts and estuaries using integrated processes model, *Ocean Eng.*, *71*, 74–95, doi:10.1016/j.oceaneng.2013.01.015.
Dissanayake, D. M. P. K., R. Ranasinghe, and J. A. Roelvink (2012), The morphological response of large tidal inlet/basin systems to relative sea level rise, *Clim. Change*, *113*, 253–276, doi:10.1007/s10584-012-0402-z.
Hagen, S. C., and P. Bacopoulos (2012), Synthetic storms contributing to coastal flooding in Florida's Big Bend Region with application to sea level rise, *Terr. Atmos. Ocean. Sci.*, *23*(5), 481–500, doi:10.3319/tao.2012.04.17.01(wmh).
Hagen, S. C., A. K. Zundel, and S. Kojima (2006), Automatic, unstructured mesh generation for tidal calculations in a large domain, *Int. J. Comput. Fluid Dyn.*, *20*(8), 593–608, doi:10.1080/10618560601046846.
Hagen, S. C., J. T. Morris, P. Bacopoulos, and J. F. Weishampel (2013), Sea-level rise impact on a salt marsh system of the lower St. Johns River, *J. Waterw. Port Coastal Ocean Eng.*, *139*(2), 118–125, doi:10.1061/(asce)ww.1943-5460.0000177.
Holgate, S. J. (2007), On the decadal rates of sea level change during the twentieth century, *Geophys. Res. Lett.*, *34*(1), doi:10.1029/2006GL028492.
Huang, W., S. Hagen, and P. Bacopoulos (2014), Hydrodynamic modeling of Hurricane Dennis impact on estuarine salinity variation in Apalachicola Bay, *J. Coastal Res.*, *30*(2), 389–398.
Huang, W., S. Hagen, P. Bacopoulos, and D. Wang (2015), Hydrodynamic modeling and analysis of sea-level rise impacts on salinity for oyster growth in Apalachicola Bay, Florida, *Estuarine Coastal Shelf Sci.*, *156*, 7–18, doi:10.1016/j.ecss.2014.11.008.
Intergovernmental Panel of Climate Change (2013), *Climate Change 2013: The Physical Science Basis. Contribution of Working Group I to the Fifth Assessment Report of the Intergovernmental Panel on Climate Change*, 1535 pp., Cambridge Univ. Press, Cambridge, UK and New York.
Irish, J., A. Sleath, M. Cialone, T. Knutson, and R. Jensen (2014), Simulations of Hurricane Katrina (2005) under sea level and climate conditions for 1900, *Clim. Change*, *122*(4), 635–649, doi:10.1007/s10584-013-1011-1.
Jevrejeva, S., J. C. Moore, and A. Grinsted (2010), How will sea level respond to changes in natural and anthropogenic forcings by 2100? *Geophys. Res. Lett.*, *37*(7), doi:10.1029/2010GL042947.
Knutson, T. R., and R. E. Tuleya (2004), Impact of CO_2-induced warming on simulated hurricane intensity and precipitation: sensitivity to the choice of climate model and convective parameterization, *J. Clim.*, *17*(18), 3477–3495, doi:10.1175/1520-0442(2004)017<3477:iocwos>2.0.co;2.
Lin, N., K. Emanuel, M. Oppenheimer, and E. Vanmarcke (2012), Physically based assessment of hurricane surge threat under climate change, *Nat. Clim. Change*, *2*(6), 462–467, doi:10.1038/nclimate1389.
McInnes, K. L., K. J. E. Walsh, G. D. Hubbert, and T. Beer (2003), Impact of sea-level rise and storm surges on a coastal community, *Nat. Hazards*, *30*(2), 187–207, doi:10.1023/a:1026118417752.
McInnes, K. L., I. Macadam, G. D. Hubbert, and J. G. O'Grady (2009), A modelling approach for estimating the frequency of sea level extremes and the impact of climate change in southeast Australia, *Nat. Hazards*, *51*(1), 115–137, doi:10.1007/s11069-009-9383-2.
Medeiros, S., S. Hagen, J. Weishampel, and J. Angelo (2015), Adjusting lidar-derived digital terrain models in coastal marshes based on estimated aboveground biomass density, *Remote Sens.*, *7*(4), 3507, doi:10.3390/rs70403507.
Morris, J. T., P. V. Sundareshwar, C. T. Nietch, B. Kjerfve, and D. R. Cahoon (2002), Responses of coastal wetlands to rising sea level, *Ecology*, *83*(10), 2869–2877, doi:10.1890/0012-9658(2002)083[2869:rocwtr]2.0.co;2.
Mousavi, M. E., J. L. Irish, A. E. Frey, F. Olivera, and B. L. Edge (2011), Global warming and hurricanes: the potential impact of hurricane intensification and sea level rise on coastal flooding, *Clim. Change*, *104*(3–4), 575–597, doi:10.1007/s10584-009-9790-0.
Needham, H. F., and B. D. Keim (2012), A storm surge database for the US Gulf Coast, *Int. J. Climatol.*, *32*(14), 2108–2123.
Needham, H. F., B. D. Keim, D. Sathiaraj, and M. Shafer (2013), A global database of tropical storm surges, *Eos Trans. AGU*, *94*(24), 213–214, doi:10.1002/2013EO240001.
Needham, H. F., B. D. Keim, and D. Sathiaraj (2015), A review of tropical cyclone-generated storm surges: global data sources, observations, and impacts, *Rev. Geophys.*, *53*(2), 545–591, doi:10.1002/2014RG000477.
Nicholls, R. J., and A. Cazenave (2010), Sea-level rise and its impact on coastal zones, *Science*, *328*(18), 1517–1520, doi:10.1126/science.1185782.
Orton, P., S. Vinogradov, N. Georgas, A. Blumberg, N. Lin, V. Gornitz, C. Little, K. Jacob, and R. Horton (2015), New York city panel on climate change 2015 report. Chapter 4: Dynamic coastal flood modeling, *Ann. N. Y. Acad. Sci.*, *1336*(1), 56–66, doi:10.1111/nyas.12589.
Parris, A., et al. (2012), Global sea level rise scenarios for the United States National Climate Assessment, *Rep.*, 37 pp., Climate Office Program (CPO), Silver Spring, Md.
Passeri, D. L., S. C. Hagen, S. C. Medeiros, and M. V. Bilskie (2015b), Impacts of historic morphology and sea level rise on tidal hydrodynamics in a microtidal estuary (Grand Bay, Mississippi), *Cont. Shelf Res.*, *111*, 150–158.
Passeri, D. L., S. C. Hagen, S. C. Medeiros, M. V. Bilskie, K. Alizad, and D. Wang (2015c), The dynamic effects of sea level rise on low-gradient coastal landscapes: a review, *Earth's Future*, *3*(6), 159–181, doi:10.1002/2015EF000298.
Passeri, D., S. Hagen, M. Bilskie, and S. Medeiros (2015a), On the significance of incorporating shoreline changes for evaluating coastal hydrodynamics under sea level rise scenarios, *Nat. Hazards*, *75*(2), 1599–1617, doi:10.1007/s11069-014-1386-y.
Passeri, D. L., S. C. Hagen, N. G. Plant, M. V. Bilskie, S. C. Medeiros and K. Alizad (2016), Tidal hydrodynamics under future sea level rise and coastal morphology in the northern Gulf of Mexico, *Earth's Future*, *4*, doi:10.1002/2015EF000332.
Pike, D., and J. Stiner (2007), Sea turtle species vary in their susceptibility to tropical cyclones, *Oecologia*, *153*(2), 471–478, doi:10.1007/s00442-007-0732-0.
Plant, N.G., E. R. Thieler and D. L. Passeri (2016), Coupling centennial-scale shoreline change to sea? level rise and coastal morphology in the Gulf of Mexico using a Bayesian network, *Earth's Future*, *4*, doi:10.1002/2015EF000331.
Powell, M. D., S. H. Houston, L. R. Amar, and N. L. Morisseau-Leroy (1998), The HRD real-time hurricane wind analysis system, *J. Wind Eng. Ind. Aerodyn.*, *77,78*, 53–64.
Reece, J., et al. (2013), Sea level rise, land use, and climate change influence the distribution of loggerhead turtle nests at the largest USA rookery (Melbourne Beach, Florida), *Mar. Ecol. Prog. Ser.*, *493*, 259–274, doi:10.3354/meps10531.

Resio, D., J. Irish, and M. Cialone (2009), A surge response function approach to coastal hazard assessment – part 1: basic concepts, *Nat. Hazards*, *51*(1), 163–182, doi:10.1007/s11069-009-9379-y.

Sleeter, B. M., et al. (2012), Scenarios of land use and land cover change in the conterminous United States: utilizing the special report on emission scenarios at ecoregional scales, *Global Environ. Change*, *22*(4), 896–914, doi:10.1016/j.gloenvcha.2012.03.008.

Smith, J. M., M. A. Cialone, T. V. Wamsley, and T. O. McAlpin (2010), Potential impact of sea level rise on coastal surges in southeast Louisiana, *Ocean Eng.*, *37*, 37–47, doi:10.1016/j.oceaneng.2009.07.008.

Solomon, J. A., M. J. Donnelly, and L. J. Walterst (2014), Effects of sea level rise on the intertidal oyster *Crassostrea virginica* by field experiments, *J. Coastal Res.*, *68*, 57–64.

Towns, J., et al. (2014), XSEDE: accelerating scientific discovery, *Comput. Sci. Eng.*, *16*(5), 62–74, doi:10.1109/mcse.2014.80.

Wang, J., W. Gao, S. Xu, and L. Yu (2012), Evaluation of the combined risk of sea level rise, land subsidence, and storm surges on the coastal areas of Shanghai, China, *Clim. Change*, *115*(3–4), 537–558, doi:10.1007/s10584-012-0468-7.

Woth, K., R. Weisse, and H. von Storch (2006), Climate change and North Sea storm surge extremes: an ensemble study of storm surge extremes expected in a changed climate projected by four different regional climate models, *Ocean Dyn.*, *56*(1), 3–15, doi:10.1007/s10236-005-0024-3.

Yang, Z., T. Wang, R. Leung, K. Hibbard, T. Janetos, I. Kraucunas, J. Rice, B. Preston, and T. Wilbanks (2014), A modeling study of coastal inundation induced by storm surge, sea-level rise, and subsidence in the Gulf of Mexico, *Nat. Hazards*, *71*(3), 1771–1794, doi:10.1007/s11069-013-0974-6.

Zhang, K., Y. Li, H. Liu, H. Xu, and J. Shen (2013), Comparison of three methods for estimating the sea level rise effect on storm surge flooding, *Clim. Change*, *118*(2), 487–500, doi:10.1007/s10584-012-0645-8.